Open Ceramics 19 (2024) 100647

Contents lists available at ScienceDirect

Open Ceramics

journal homepage: www.sciencedirect.com/journal/open-ceramics

The reactivity of α-tricalcium phosphate powders is affected by minute amounts of β-calcium pyrophosphate and by the synthesis temperature

Marc Bohner *, Fabrizio Bigolin, Isabelle Bohner, Thomas Imwinkelried, Yassine Maazouz, Pascal Michel, Christoph Stähli, Yves Viecelli, Nicola Döbelin

RMS Foundation, Bischmattstrasse 12, CH-2544, Bettlach, Switzerland

ARTICLE INFO

Handling editor: Jens Guenster

Keywords:
Powder
Synthesis
Phase diagram
Bone
Setting

ABSTRACT

α-tricalcium phosphate (α-TCP) is the most widespread raw material for hydraulic calcium phosphate cements (CPCs). CPCs are widely used in bone repair due to their injectability, setting ability, and osteoconductivity. This study investigated the reactivity of α-TCP powders, focusing on the impact of minor phase impurities, β-calcium pyrophosphate and hydroxyapatite, and the synthesis temperature. The α-TCP powders were synthesized via a solid-state reaction of calcium carbonate and anhydrous dicalcium phosphate, with varying Ca/P molar ratios (1.4850–1.5075) and synthesis temperatures (1175°C–1350 °C). Powders produced with a Ca/P molar ratio below 1.50 and synthesized at a temperature above the melting point of β-CPP (1296 °C) had a broader size distribution and a two to fourfold lower hydraulic reactivity. Conversely, a higher Ca/P molar ratio improved reactivity. The study underscores the importance of precise control over synthesis parameters to enhance the performance of α-TCP-based CPCs, offering insights for optimizing material design in biomedical applications.

1. Introduction

α-tricalcium phosphate (α-TCP; α-$Ca_3(PO_4)_2$) powder is used as a raw material for the production of hydraulic calcium phosphate cements (CPCs) [1,2]. Upon mixing with an aqueous solution, α-TCP particles dissolve and crystals of calcium-deficient hydroxyapatite (CDHA; $Ca_9(HPO_4)(PO_4)_5OH$) precipitate [3]. At a low enough liquid-to-powder ratio (LPR), CDHA crystals get entangled during their growth, thereby stiffening the α-TCP-based aqueous paste and providing mechanical stability. The reaction can be written [3]:

$$3\ \alpha\text{-}Ca_3(PO_4)_2 + H_2O \rightarrow Ca_9(HPO_4)(PO_4)_5OH \quad (1)$$

Since CDHA is very similar in its composition and structure to bone mineral, α-TCP-based CPCs have been extensively used for the repair of bone defects [2]. Their main advantage compared to other types of bone graft substitutes (BGS) is their ability to be injected and to harden, thus providing a temporary though fragile fixation of the bone defect. The osteoclast-mediated resorption process of CDHA enables a smooth conversion of a cement-filled defect into regenerated bone [4]. Clinical indications include the treatment of tibia plateau fractures [5], distal radius fractures [2,6], and the reinforcement of osteoporotic bone [7].

Various studies have investigated the effect of α-TCP powder properties on the physico-chemical properties of α-TCP-based CPCs. These studies have revealed that cement pastes made with finer α-TCP powders are more injectable [8,9], more cohesive [10], and react faster [9–11]. After hardening, the cements have a finer microstructure than the α-TCP powder bulk [10,12], meaning that the specific surface area is higher, and the pores are smaller [12].

There are numerous studies devoted to the effect of additives on the hydraulic properties of α-TCP-based CPCs, but surprisingly few studies have addressed the effect of chemical impurities present in the α-TCP powder on the physico-chemical properties of the cements. The most investigated effect is related to the presence of amorphous calcium phosphate (ACP) phases produced during α-TCP powder milling. During the hydraulic reaction of an ACP-rich α-TCP powder, ACP was observed to be the first phase to react [13]. Thermally treating the α-TCP powders at 500 °C for 1–24 h led to ACP disappearance and accordingly to a strong decrease in reactivity [9,13–16]. To our knowledge, no study has been devoted to the effect of other phase impurities present in α-TCP powders, namely β-calcium pyrophosphate (β-CPP; β-$Ca_2P_2O_7$), β-tricalcium phosphate (β-TCP; β-$Ca_3(PO_4)_2$), and hydroxyapatite (HA; $Ca_5(PO_4)_3OH$). However, it must be added that HA nano powders are often added to α-TCP-based cements to act as seeding material, thereby accelerating the setting reaction [16,17].

* Corresponding author.
E-mail address: marc.bohner@rms-foundation.ch (M. Bohner).

https://doi.org/10.1016/j.oceram.2024.100647
Received 14 June 2024; Accepted 18 July 2024
Available online 26 July 2024

Table 1
Composition of the CC-DCP mixtures used to obtain the targeted Ca/P molar ratios of the α-TCP batches. The compositions are adjusted to consider the presence of water in the raw materials and the evaporation of phosphor-species during sintering. The expected β-CPP and HA content is listed in the last two columns of the table.

Targeted Ca/P molar ratio	CC amount [g]	DCP amount [g]	Expected β-CPP content [wt %]	Expected HA content [wt %]
1.4850	32.90	99.10	2.4 %	–
1.4900	33.17	98.83	1.6 %	–
1.4950	33.44	98.56	0.8 %	–
1.5000	33.71	98.29	–	–
1.5025	33.85	98.15	–	1.6 %
1.5050	33.98	98.02	–	3.2 %
1.5075	34.12	97.88	–	4.9 %

Table 2
Phase-specific crystallographic constants used for the calculation of absolute phase quantities. "pfu" stands for "per formula unit".

Phase	PDF-4+ database record	Mass absorption coefficient [cm^2/g]	Molar mass [g/mol]	Mol Ca pfu	Mol P pfu
α-TCP	04-010-4348	85.72296272	310.1767	3	2
β-TCP	04-008-8714	85.72296272	310.1767	3	2
HA	01-074-0565	86.54987704	502.3114	5	3
β-CPP	04-009-3876	77.10324026	254.0993	1	1
α-Al_2O_3	04-004-2852	31.66443804	–	–	–

In recent years, various studies have shown that <5 % variations of the Ca/P molar ratio of β-TCP powders can affect β-TCP crystallographic structure [18], sintering rate [19], and osteoclastic resorption rate [19]. These results are particularly relevant for the biomedical field since international standards consider that calcium phosphate materials (including α-TCP, β-TCP and HA) can be called "phase pure" with >95 % crystalline phase purity. In this study, it was hypothesized that minor variations of the Ca/P molar ratio of α-TCP strongly modify α-TCP physico-chemical properties. The aim was therefore to produce α-TCP powders with <5 % β-CPP and HA impurities and assess the effect of these phase impurities on the physico-chemical properties of α-TCP powders and α-TCP-based CPC. A particular attention was paid to the interaction between the β-CPP content and α-TCP synthesis temperature since the high-temperature β-CPP phase, α-CPP, melts at 1296 °C [20], a temperature often below the temperature used to produce α-TCP [21]. The main measurable considered here was the reactivity of the powder.

Two main methods can be used to produce α-TCP: a solid-state reaction or the phase-transformation of CDHA [22]. Considering the aim of this study, it was decided to produce α-TCP by solid-state reaction of calcium carbonate (CC; $CaCO_3$) and anhydrous dicalcium phosphate (DCP; $CaHPO_4$) according to the reaction:

$$CaCO_3 + 2\ CaHPO_4 \rightarrow \alpha\text{-}Ca_3(PO_4)_2 + H_2O + CO_2 \quad (2)$$

The content of β-CPP and HA was controlled with a small excess of DCP or CC, respectively.

2. Materials and methods

2.1. Production of α-TCP powder

The method used to produce α-TCP has been described in the past [14]. A mixture containing a 2:1 ratio of CC (VWR, Belgium, product number 22300.290) and DCP (Jost, Poland, Product number 2278) was uniformly blended 10 min in a Turbula T2F mixer (Bachofen, Switzerland). This mixture was then subjected to calcination at 900 °C for 1 h in an LH60/14 furnace (Nabertherm, Germany), followed by cooling to ambient temperature. Subsequently, the material was given on a sieve with 0.5 mm openings. After calcination and sieving, the powder was sintered at 1350 °C for 4 h before being air-quenched in air upon removal from the furnace at 1240 °C. The sintered material was then processed in a jaw crusher (model BB51 by Retsch, Germany) until it was fine enough to pass through a 2 mm sieve. The final step involved ball milling the powder in a planetary mill (model Pulverisette 5 by Fritsch, Germany) at a speed of 400 revolutions per minute for 15 min in zirconia containers. The zirconia spheres were removed with a 5.6 mm sieve and the milled powder was then dried at 60 °C to a constant weight and sieved with a 0.125 mm sieve.

Since phosphor species evaporate during sintering [23], a 1:2 M ratio between CC and DCP content does not lead to 100 % α-TCP. As a result, a first batch was produced to determine the gap between the expected and the obtained Ca/P molar ratio of the α-TCP powder. This difference of composition was then used to adjust the Ca/P molar ratio of the subsequent powders. Targeted Ca/P molar ratios were 1.4850, 1.4900, 1.4950, 1.5000, 1.5025, 1.5050, and 1.5075 (Table 1). In a second step, the synthesis temperature was lowered from 1350 °C to 1250 °C, 1200 °C, and 1175 °C for four α-TCP powder compositions, namely 1.4900, 1.4950, 1.5025, and 1.5050.

2.2. X-ray diffraction analysis

The crystalline phase composition was determined by X-ray powder diffraction (XRD) using an external standard for absolute phase quantification. Samples previously milled in the planetary mill were measured without further processing, other samples were milled for 3 min in isopropanol (>99 %) using the McCrone Micronizing Mill (Retsch GmbH, Haan, Germany) with zirconia milling aids. XRD patterns were recorded on a Bruker D8 Advance diffractometer (Bruker AXS GmbH, Karlsruhe, Germany) in θ–θ geometry using CuKα radiation filtered with an Ni-filter and an energy-dispersive detector. A range from 4.0 to 80.0 °2θ was scanned with a step-size of 0.0122 °2θ and a counting time of 0.5 s per step. An external standard sample (NIST SRM676a Al_2O_3) was measured using identical instrument settings at the beginning of each measurement series, half way through the series, and at the end of the series. These datasets were used to correct the measured intensities for tube intensity fluctuations during the data collection series, as well as for the 100 % crystallinity reference intensity.

All datasets were processed with Rietveld refinement using the software Profex version 4–5 with the Rietveld refinement kernel BGMN [24]. Crystal structure models were taken from the ICDD PDF-4+ database version 2021 [https://www.icdd.com] as listed in Table 2. Cell parameters, an isotropic scale factor, and crystallite-size related peak broadening were refined for all phases. For the strongest phase (α-TCP and Al_2O_3, respectively), a texture model using spherical harmonics of the 6th order, as well as bimodal crystallite sizes and micro-strain were also refined. Atomic coordinates and thermal displacement parameters were fixed at their published values for all phases. If an unambiguous signal of HA was observed, β-CPP was removed from the refinement, and vice-versa, because thermodynamics exclude their coexistence in homogeneous thermally equilibrated samples. An example refinement is shown in Fig. 1b.

The external standard approach for absolute phase quantification required the determination of the samples' mass absorption coefficients (MAC). Due to the low amount of amorphous content that were anticipated in the samples, and the expected chemical similarity of the amorphous phase with the crystalline phases, the sample MACs were calculated from the crystalline phase composition only, ignoring the potential presence of an amorphous phase. Phase MACs listed in Table 2 were calculated from the structure models by the Rietveld refinement software based on absorption data taken from [https://physics.nist.gov/PhysRefData/FFast/html/form.html].

Prior to phase normalization, the refinement software reported a phase scale factor G, which is already corrected for the density of the unit cell (Eq (2)):

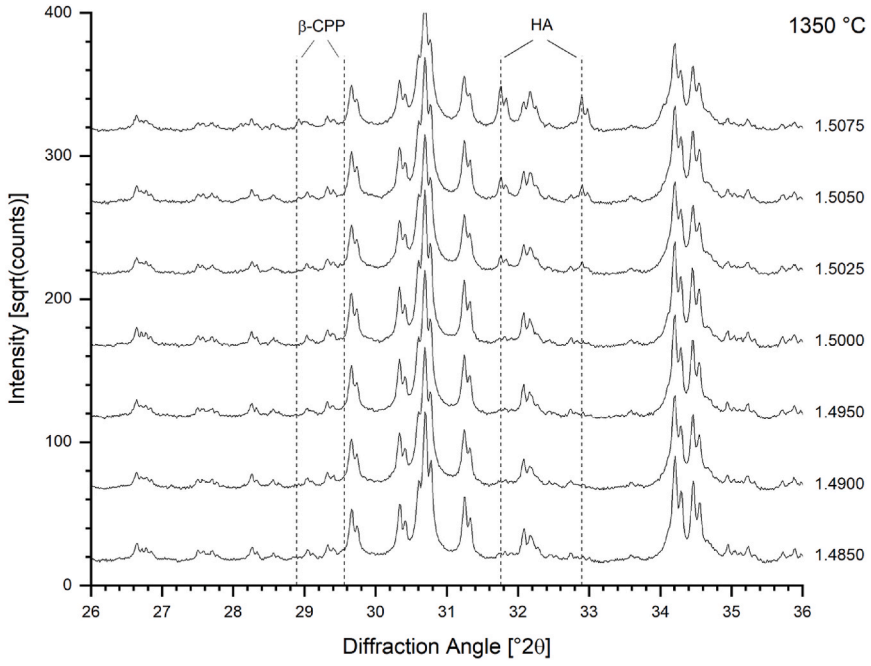

(a)

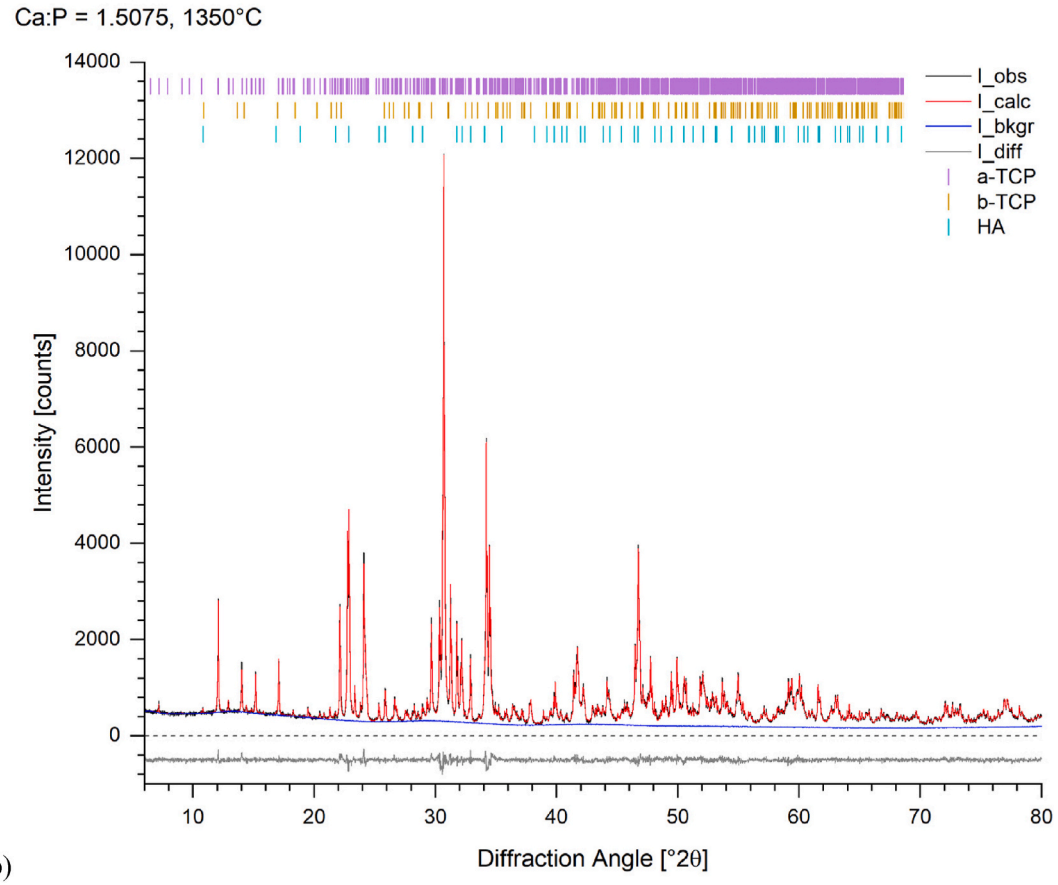

(b)

Fig. 1. (a) XRD patterns of samples processed at 1350 °C contained a weak signal of β-CPP if the Ca:P ratio was below 1.50, and a more pronounced signal of HA if the Ca:P ratio was greater than 1.50. The vertical axis shows the square root of the raw intensities to enhance the visibility of signals at the background level. The positions of the strongest non-overlapping β-CPP and HA peaks are marked by dashed lines. (b) All Rietveld refinements resulted in high qualities of fits, as documented by the representative refinement of the sample with a Ca/P molar ratio of 1.5075 processed at 1350 °C.

Table 3
Summary of the XRD results in weight fractions. The estimated standard deviation (ESD) of the measured values reported by the Rietveld refinement software is indicated for each phase. The "measured Ca/P ratio" is the molar ratio calculated from the phase composition assuming that the amorphous phase has a Ca/P molar ratio of 1.50.

Expected				Phase composition										Measured	
Ca/P ratio	Sinter T /°C	Crystallinity	ESD	α-TCP	ESD	β-TCP	ESD	β-CPP	ESD	HA	ESD	ACP	ESD	Ca/P ratio	ESD
1.4900	1175	92.6%	0.3%	90.3%	0.3%	0.7%	0.1%	1.6%	0.1%	0.0%	0.0%	7.4%	0.3%	1.4893	0.0004
1.4950	1175	95.0%	0.3%	93.2%	0.3%	0.8%	0.1%	1.1%	0.1%	0.0%	0.0%	5.0%	0.3%	1.4931	0.0004
1.5025	1175	91.4%	0.3%	90.3%	0.3%	0.6%	0.1%	0.3%	0.1%	0.2%	0.0%	8.6%	0.3%	1.4982	0.0004
1.5050	1175	92.9%	0.3%	91.2%	0.3%	0.9%	0.1%	0.1%	0.1%	0.7%	0.0%	7.2%	0.3%	1.5005	0.0004
1.4900	1200	96.4%	0.4%	94.6%	0.3%	0.3%	0.1%	1.5%	0.1%	0.0%	0.0%	3.6%	0.4%	1.4906	0.0004
1.4950	1200	94.8%	0.3%	93.6%	0.3%	0.3%	0.0%	0.9%	0.1%	0.0%	0.0%	5.2%	0.3%	1.4943	0.0004
1.5025	1200	97.0%	0.3%	96.5%	0.3%	0.3%	0.1%	0.3%	0.1%	0.0%	0.0%	3.0%	0.3%	1.4984	0.0004
1.5050	1200	95.4%	0.3%	94.0%	0.3%	0.2%	0.1%	0.2%	0.1%	0.9%	0.0%	4.6%	0.3%	1.5002	0.0005
1.4900	1250	92.7%	0.3%	91.0%	0.3%	0.3%	0.1%	1.4%	0.1%	0.0%	0.0%	7.3%	0.3%	1.4909	0.0004
1.4950	1250	89.1%	0.3%	88.0%	0.3%	0.3%	0.1%	0.8%	0.1%	0.0%	0.0%	10.9%	0.3%	1.4946	0.0004
1.5025	1250	94.2%	0.3%	92.2%	0.3%	0.2%	0.1%	0.4%	0.1%	1.4%	0.0%	5.8%	0.3%	1.4999	0.0004
1.5050	1250	94.4%	0.3%	92.1%	0.3%	0.4%	0.1%	0.4%	0.1%	1.6%	0.0%	5.6%	0.3%	1.5001	0.0006
1.4850	1350	90.2%	0.3%	88.7%	0.3%	0.2%	0.1%	1.3%	0.1%	0.0%	0.0%	9.8%	0.3%	1.4914	0.0004
1.4900	1350	92.3%	0.3%	91.1%	0.3%	0.3%	0.1%	0.9%	0.1%	0.0%	0.0%	7.7%	0.3%	1.4939	0.0004
1.4950	1350	91.7%	0.3%	91.1%	0.3%	0.0%	0.0%	0.5%	0.1%	0.0%	0.0%	8.3%	0.3%	1.4966	0.0004
1.5000	1350	95.1%	0.3%	94.5%	0.3%	0.2%	0.1%	0.4%	0.1%	0.0%	0.0%	5.0%	0.3%	1.4977	0.0006
1.5025	1350	96.0%	0.3%	94.2%	0.3%	0.2%	0.1%	0.3%	0.1%	1.3%	0.0%	4.0%	0.3%	1.5000	0.0005
1.5050	1350	97.1%	0.3%	94.2%	0.3%	0.2%	0.1%	0.2%	0.1%	2.5%	0.0%	2.9%	0.3%	1.5026	0.0004
1.5075	1350	96.3%	0.3%	88.3%	0.3%	0.4%	0.1%	0.1%	0.1%	7.5%	0.1%	3.7%	0.3%	1.5115	0.0004

$$G = S \cdot (Z \cdot M \cdot V) \tag{2}$$

S is the refined Rietveld scale factor, Z is the number of formula units per unit cell, M is the molar mass of the formula unit, and V is the cell volume [25]. This corrected phase scale factor G was further used to determine absolute phase quantities. First, the crystallinity ratio C of the sample was determined by comparing the sum of all CaP scale factors, corrected for the mass absorption coefficient, with the corresponding value of the external Al_2O_3 standard according to Eq. (3):

$$C\ [\%] = 100 \cdot \frac{\sum (G_i \cdot MAC_i)}{G_{std} \cdot MAC_{std}} \tag{3}$$

Afterwards, the absolute phase quantities Q and the amorphous content A were obtained according to Eqs. (4) and (5):

$$Q\ [\text{wt-}\%] = C \cdot \frac{G}{\sum G_i} \tag{4}$$

$$A\ [\text{wt-}\%] = 100 - \sum Q_i \tag{5}$$

The molar Ca:P ratios were calculated for the crystalline fractions of the samples according to Eq. (6) using the data listed in Table 2:

$$Ca:P = \frac{\sum \left(nCa \cdot \frac{Q}{M} \right)_i}{\sum \left(nP \cdot \frac{Q}{M} \right)_i} \tag{6}$$

nCa and nP are the numbers of Ca and P ions per formula unit, respectively, and M is the molar mass.

2.3. Scanning electron microscopy

For the scanning electron microscopy (SEM) observations of the powders, a conductive carbon adhesive disc (Agar scientific code AGG3347 N) was glued on an aluminum SEM sample holder. Using a thin spatula, a small quantity of powder was placed on the carbon pad. Excess powder was removed by careful tapping and the use of filtered compressed air. The samples were then sputtered with gold (45–50 s, 30 mA) in a compact coating unit (safematic, CCU-010). SEM images were taken using the secondary electron detector at an electron high voltage (EHT) of 5 kV and a working distance of ca. 8 mm (ZEISS Sigma 300 VP, Carl Zeiss Microscopy, Oberkochen, Germany).

For the SEM observation of the cement microstructure (materialography samples), the following procedure was followed. Fragments of the cements were placed in a Polypropylene casting mold and embedded in epoxy resin (Struers Epofix resin and hardener, ratio 25:3) under vacuum (Struers CitoVac). Before mixing with the hardener, the resin was slightly heated to decrease its viscosity. After the impregnation, the embedded sample was placed in a refrigerator at 4 °C for 4h. Then the sample was hardened overnight at room temperature. Grinding and polishing were performed manually on a "Presi, Mecatech 334" polishing machine (Presi Sarl, Le Locle, Switzerland). Isopropanol was used as a lubricant in every grinding and polishing step. For the grinding steps (P320, P500, P1200) SiC paper was used. Grinding was performed at 300 rpm for 10–30 s each. Between the grinding steps, samples were cleaned in Isopropanol using ultrasound. The polishing process included 6 μm, 3 μm (Diamond) on woven polishing cloth discs (Struers MD-DAC and MD-DUR). For final polishing a few drops of 0.2 μm silica suspension, water-free, (AKASEL Nr. Oxipol-010) was given on a neoprene polishing disc (Struers MD-CHEM). The polishing time was 2–4 min for each step. The embedded samples were glued on an aluminum SEM sample holder, a thin line of silver paint was drawn around the surface and connected to the aluminum sample holder. The samples were then coated with carbon (50 s) in a compact coating unit (safematic, CCU-010). SEM images were taken, using the BSE detector at EHT 10 kV and a working distance of ca. 8 mm (SEM, ZEISS Sigma 300 VP).

2.4. Particle size distribution

Particle size distributions (PSD) were measured using laser diffraction (LS 13320, Beckmann Coulter Indianapolis, USA) with the Tornado Dry Power System (DPS). The powder was sampled with a scoop three times after manual tumbling of the wide mouth bottles. Three samples of about 10 mL volume were tested for each parameter setting. The dry powder was dispersed within the Tornado DPS and passed the

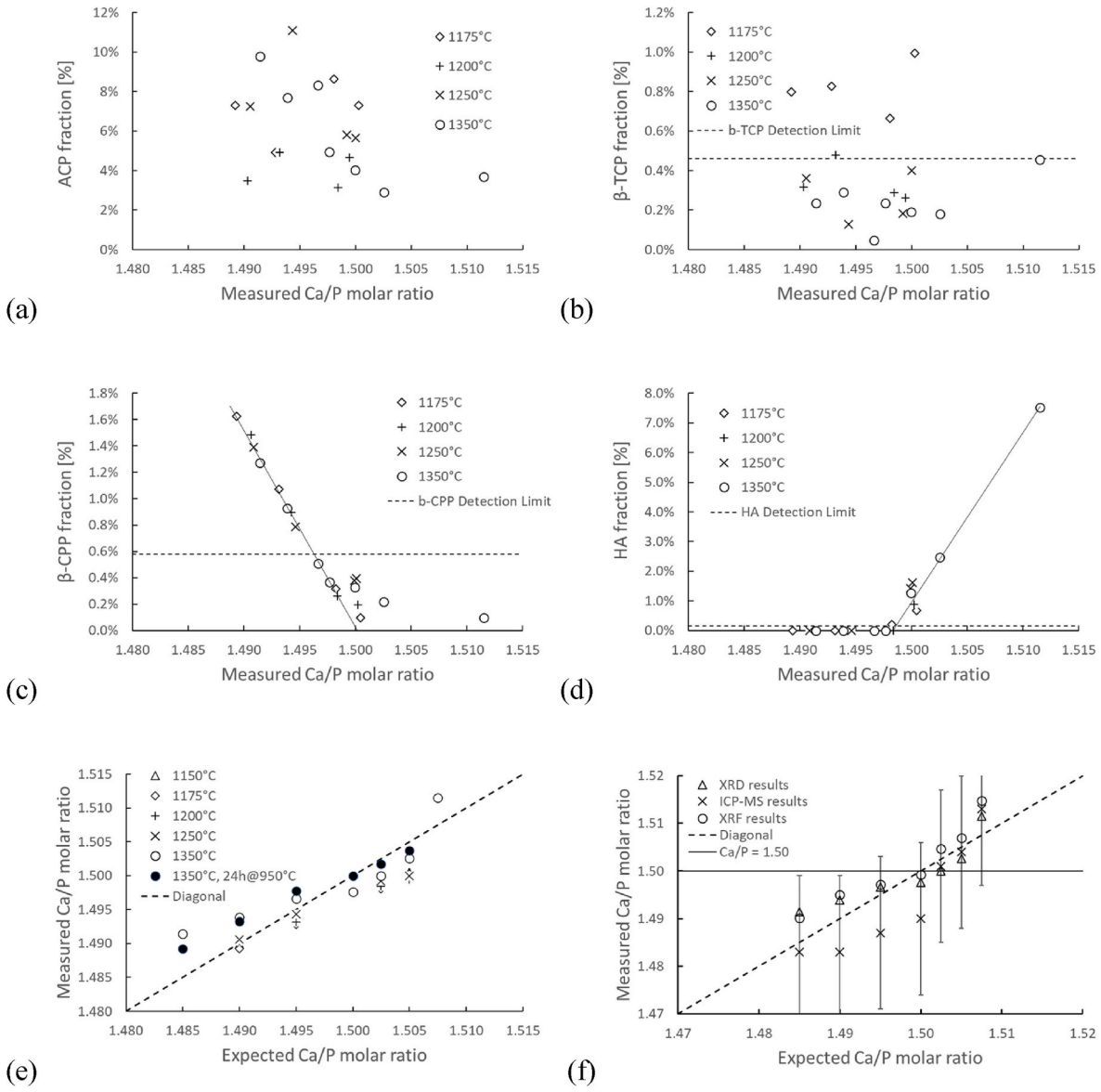

Fig. 2. Quantitative results of the Rietveld refinement analysis of the XRD data showing the effect of the measured Ca/P molar ratio on the fraction of (a) ACP, (b) β-TCP, (c) β-CPP, (d) and HA in α-TCP powders. The relationship between the expected and measured Ca/P molar ratio is shown in (e). Part (f) reports the Ca/P molar ratios determined by XRF, XRD and ICP-MS. In (e), the Ca/P molar ratio of the powder synthesized at 1350 °C was calculated twice, once directly on the α-TCP powder after production, and once after calcining the powder during 24h at 950 °C. The errors on the ICP-MS results given in (f) correspond to the uncertainty of the methods as calculated during a method validation performed for an ISO 17025 accreditation.

measurement chamber where monochromatic light with a wavelength of 780 nm was used as main illumination source. The scattering patterns were recorded by 126 detectors placed at angles up to 35° from the optical axis. The Mie theory was applied with a real refractive index of 1.0 for air and of 1.60 for the powder. The complex refractive index was set to 0. Spherical particles with smooth, homogenous surface were assumed. Based on this assumption, volume and number distributions and the specific surface area (SSA) were calculated. For the determination of the d-values, a logarithmic normal distribution was assumed.

2.5. Inductively coupled plasma-mass spectrometry

The second of the three methods used to determine the Ca/P molar ratio of the α-TCP powders is inductively coupled plasma-mass spectrometry (ICP-MS; Agilent 7700x, Agilent Technologies, Santa Clara, USA). The powders were dissolved in 69 % HNO_3 (w/w) and diluted 1:1000 in a solution of demineralized H_2O containing 3 % HNO_3, 2 % HCl and 0.01 % HF (all: Rotipuran® Supra, Carl Roth, Karlsruhe, Germany). ^{44}Ca and ^{31}P signals measured in the solutions were calibrated against a custom-made certified standard solution containing Ca and P ions in a molar ratio of 1.55 (Inorganic Ventures, Christiansburg, USA). Signals of trace impurity elements were calibrated against multi-element standard solutions (Inorganic Ventures). Calibration drifts were corrected according to the Ca–P standard measured after every 8th sample and according to a 20-ppb internal Sc standard solution (Inorganic Ventures, USA) measured along with each sample. Finally, the mean values of four measurements per sample were determined.

2.6. Isothermal calorimetry

A TAM Air Cement isothermal calorimeter (Thermometric AB, Sweden), equipped with 8 distinct measuring cells, was utilized to examine the heat exchange process during and post-mixing of a calcium phosphate powder blend with 1 mL of an aqueous solution. For the

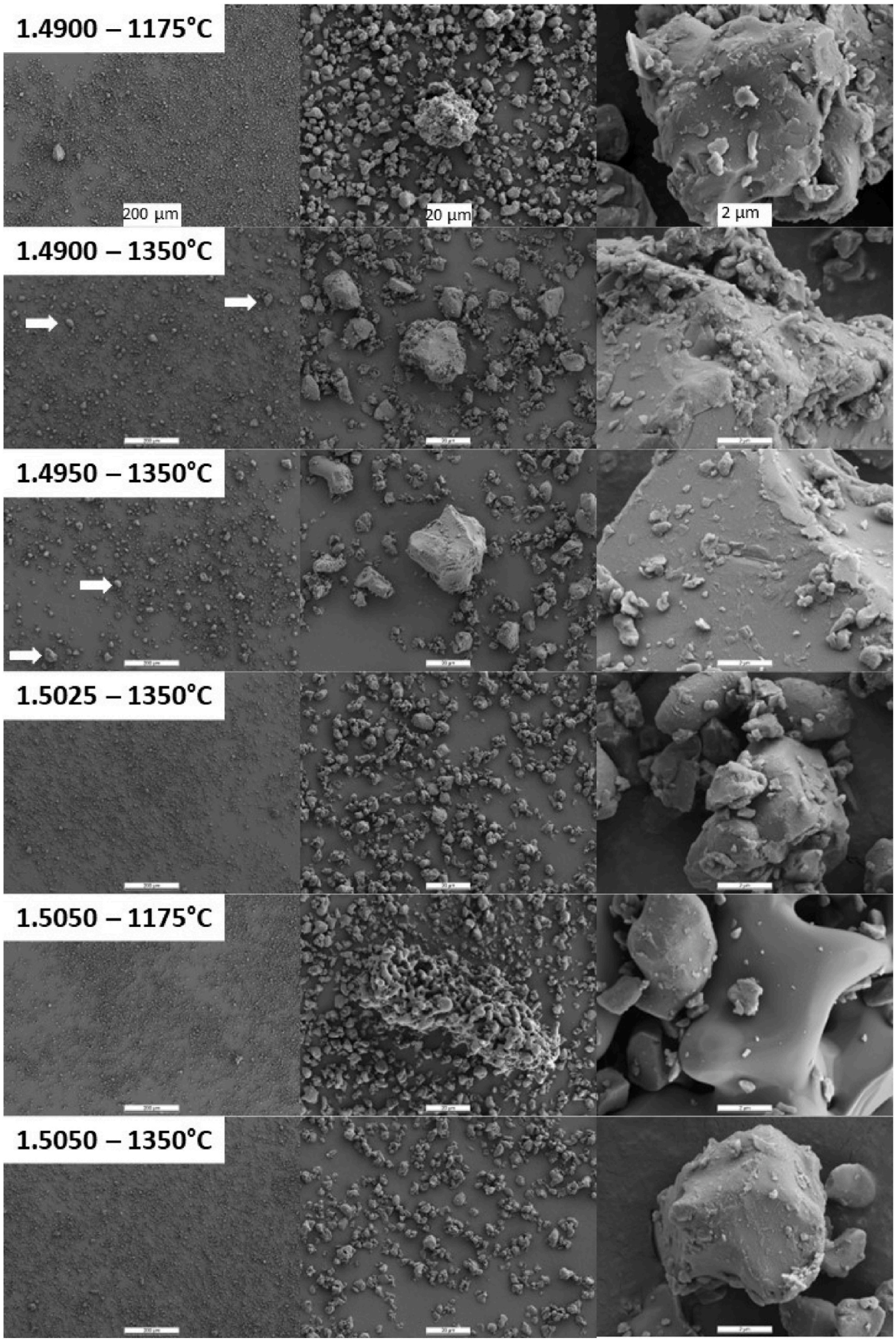

Fig. 3. SEM images of α-TCP powders produced at 1175 °C or 1350 °C and with different nominal Ca/P molar ratios. Three enlargements are shown per powder. The scale bars have a width of 200, 20, and 2 µm, respectively (from left to right). Large dense agglomerates are shown with a white arrow.

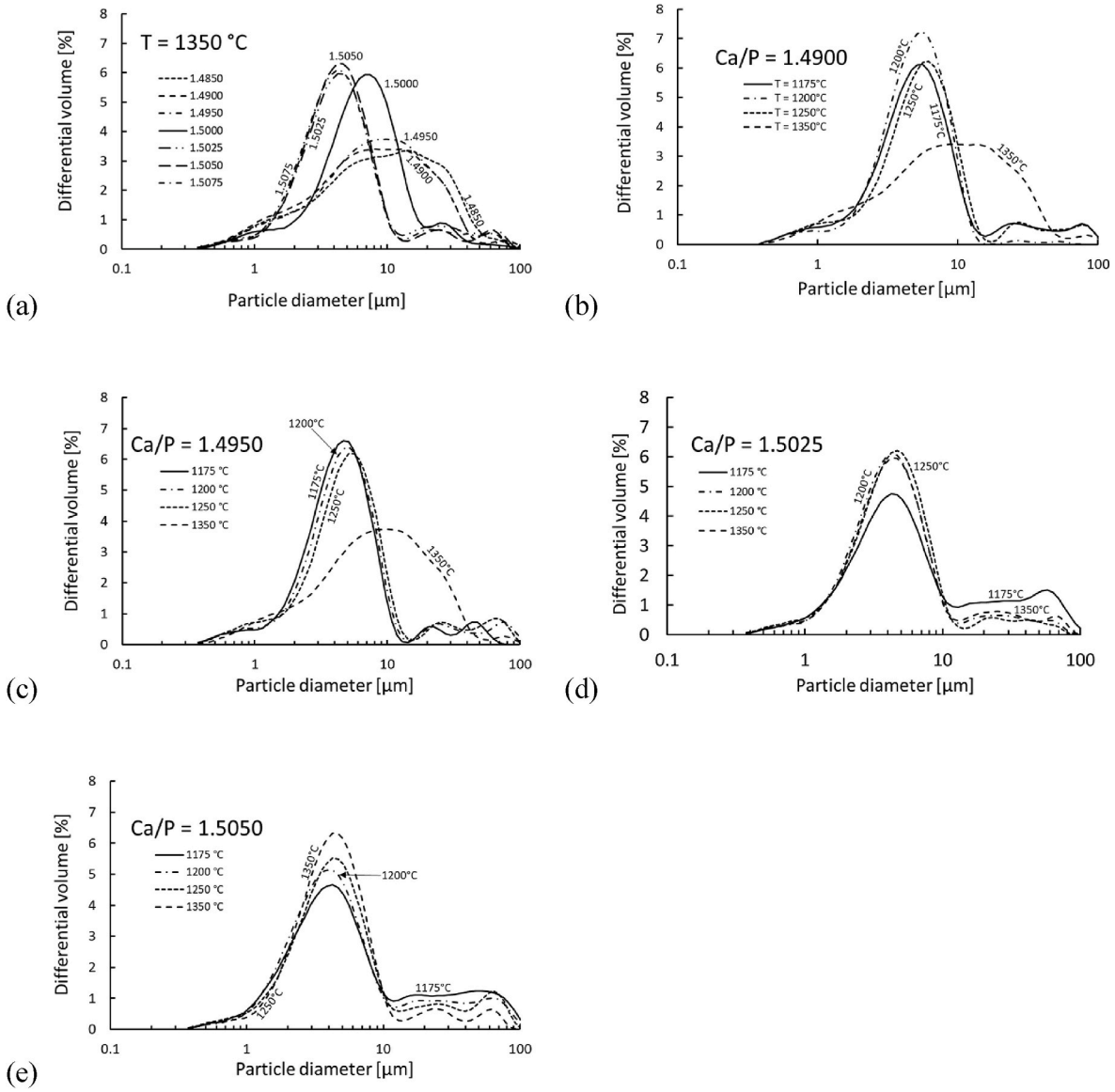

Fig. 4. Particle size distribution in volume of α-TCP powders produced (a) at 1350 °C and different nominal Ca/P ratios, or (b, c, d, e) at different temperatures and a nominal Ca/P molar ratio of 1.490, 1.495, 1.5025, and 1.505, respectively.

experiments, 2.0g α-TCP powder, along with 1.0 mL of the solution, were introduced into the sealed compartments of the mixing cell (referred to as the "20 mL Admix Ampoule"), all maintained at a temperature of 37 °C. Subsequently, the mixing cell was inserted into the calorimeter. Upon reaching a constant (zero) signal, typically after 75–90 min, the solution was injected into the powder and thoroughly mixed using a mixing rod. The measurements were concluded once a steady thermal signal was achieved, typically within 7 days. Each composition underwent four to five randomized repetitions for robustness.

2.7. Wavelength dispersive X-ray fluorescence

The third of the three methods used to determine the Ca/P molar ratio of the α-TCP powders is wavelength dispersive X-ray fluorescence (WD-XRF; S8 Tiger, Bruker, Germany). For that purpose, certified primary standards consisting of lithium phosphate (Li_3PO_4) and calcium carbonate ($CaCO_3$) were used to calibrate the instrument. The calcium carbonate was annealed beforehand at 1200 °C to create a stable compound of CaO. A total of 13 reference samples were prepared to produce the calibration samples using a molar Ca/P molar ratio of 0.500–2.000. In the process, 1 g of sample material (mixture of Li_3PO_4 and CaO) was fused with 9 g of lithium tetraborate ($Li_2B_4O_7$) in a platinum crucible in a Leneo electric furnace from Claisse (Malvern Panalytical) at 1065 °C to form a homogeneous glass melting tablet. The same mixing ratio was used to measure the test samples as for the calibration samples (1 g sample material and 9 g $Li_2B_4O_7$).

3. Statistics

ANOVA was performed using a general linear model in order to identify the significant effect ($p < 0.01$) of the factors considered on the measured responses. Tukey pairwise comparison was used in order to identify the significant differences between groups ($p < 0.01$). The program Minitab 19 (Minitab LLC) was used for that purpose.

4. Results

All powders were essentially crystalline (Fig. 1a) even though the internal Al_2O_3 standard revealed that they contained a small amount

Table 4
Summary of the particle size distribution results. The first column contains the expected or targeted Ca/P molar ratio. The average d-values are given in μm ± the standard deviation. The values d10, d50 and d90 correspond to 10 %, 50 % and 90 % on the cumulated distribution curves, either as a function of the particle volume or the particle number. The last column contains the SSA values determined by nitrogen adsorption (BET method).

		Particle Size Distribution (Volume)			Particle Size Distribution (Number)			SSA
Ca/P ratio	Sinter T /°C	d10	d50	d90	d10	d50	d90	
1.4900	1175	1.92 ±0.04	4.93 ±0.03	19.1 ±4.78	0.427 ±0.001	0.630 ±0.006	1.68 ±0.04	1.92 ±0.01
1.4950	1175	2.02 ±0.01	4.70 ±0.03	10.0 ±0.35	0.425 ±0.000	0.621 ±0.002	1.91 ±0.01	1.67 ±0.02
1.5025	1175	1.90 ±0.02	5.24 ±0.12	46.0 ±1.70	0.436 ±0.002	0.693 ±0.008	2.00 ±0.02	2.35 ±0.02
1.5050	1175	1.81 ±0.02	4.96 ±0.11	44.3 ±2.53	0.440 ±0.003	0.744 ±0.023	2.10 ±0.03	2.34 ±0.01
1.4900	1200	2.10 ±0.04	4.72 ±0.11	8.5 ±0.55	0.424 ±0.001	0.611 ±0.006	1.89 ±0.04	1.39 ±0.04
1.4950	1200	2.07 ±0.01	5.03 ±0.08	17.7 ±5.63	0.428 ±0.002	0.631 ±0.007	1.78 ±0.02	1.72 ±0.03
1.5025	1200	1.91 ±0.03	4.46 ±0.13	14.9 ±4.83	0.429 ±0.003	0.656 ±0.005	2.18 ±0.03	1.62 ±0.02
1.5050	1200	1.83 ±0.02	4.55 ±0.08	34.0 ±1.09	0.440 ±0.001	0.772 ±0.014	2.26 ±0.04	1.82 ±0.01
1.4900	1250	1.89 ±0.03	5.37 ±0.10	18.5 ±6.27	0.431 ±0.004	0.644 ±0.017	1.46 ±0.05	1.87 ±0.02
1.4950	1250	1.94 ±0.07	5.36 ±0.16	20.2 ±6.57	0.435 ±0.003	0.659 ±0.014	1.56 ±0.06	1.86 ±0.05
1.5025	1250	1.87 ±0.02	4.58 ±0.09	10.7 ±1.25	0.430 ±0.003	0.652 ±0.014	1.98 ±0.03	1.70 ±0.02
1.5050	1250	1.89 ±0.03	4.76 ±0.11	31.3 ±3.69	0.432 ±0.003	0.673 ±0.012	2.06 ±0.04	2.03 ±0.01
1.4850	1350	1.89 ±0.05	9.62 ±0.34	31.9 ±0.48	0.451 ±0.003	0.728 ±0.011	1.54 ±0.03	1.24 ±0.03
1.4900	1350	1.75 ±0.04	8.23 ±0.21	27.2 ±1.39	0.451 ±0.005	0.731 ±0.020	1.56 ±0.05	1.49 ±0.02
1.4950	1350	1.98 ±0.04	8.64 ±0.20	26.6 ±1.28	0.455 ±0.010	0.741 ±0.030	1.60 ±0.06	1.24 ±0.02
1.5000	1350	2.45 ±0.02	6.86 ±0.03	15.5 ±0.26	0.451 ±0.005	0.718 ±0.015	1.65 ±0.03	1.09 ±0.02
1.5025	1350	1.94 ±0.03	4.61 ±0.08	19.7 ±1.71	0.431 ±0.001	0.662 ±0.007	2.15 ±0.04	1.58 ±0.03
1.5050	1350	2.00 ±0.03	4.51 ±0.09	12.2 ±2.64	0.430 ±0.001	0.666 ±0.013	2.31 ±0.07	1.49 ±0.02
1.5075	1350	1.91 ±0.05	4.42 ±0.11	14.9 ±3.67	0.430 ±0.001	0.662 ±0.007	2.20 ±0.03	1.75 ±0.03

(3–11 %) of an amorphous calcium phosphate phase (ACP; Table 3; Fig. 2a). Except for the powders synthesized at 1175 °C, all β-TCP contents were below the limit of detection (Fig. 2b). There was no apparent relationship between the content of ACP and β-TCP, and the Ca/P molar ratio (Fig. 2a and b). Decreasing the overall Ca/P molar ratio increased the fraction of β-CPP (Fig. 2c). Similarly, an increase of the Ca/P molar ratio led to an increase of the HA content (Fig. 2d). Both effects were linear. The dispersion of the measured Ca/P molar ratios of all the powders produced at one given expected Ca/P molar ratio was small, demonstrating the reproducibility of the synthesis method (Fig. 2e). The powders produced with an expected Ca/P ratio of 1.4950 had a significantly different composition than the powders produced with an expected Ca/P molar ratio of 1.5025 ($p = 0.0008$). The XRF and ICP-MS data obtained on the powders produced at 1350 °C confirmed the validity of the calculations made by Rietveld refinement of the XRD data (Fig. 2f).

The SEM images of the α-TCP powders revealed that most particles had a diameter in the range of 1–10 μm (Fig. 3, Fig. S1). Agglomerates were present in all powders, but only the agglomerates in powders produced with a Ca/P molar ratio below 1.50 and a synthesis temperature of 1350 °C appeared particularly dense and numerous. The observations made on the SEM images (Fig. 3) were confirmed by the PSD values gathered by dynamic light scattering (Fig. 4; Table 4).

The PSDs in volume of the powders demonstrated that most of the powders consisted of particles with a diameter close to 5–10 μm and agglomerates up to 120 μm (Fig. 4). Accordingly, the d50 values were all between 4.4 and 9.6 μm (Table 4). However, the powders produced at a synthesis temperature of 1350 °C and a Ca/P molar ratio below 1.50 had d50 values roughly twice larger than those of the other powders (Fig. 5c, Table 4). A *t*-test revealed that the difference was significant at $p = 0.008$. A 2-way ANOVA analysis using 4 Ca/P molar ratios (1.49, 1.495, 1.5025, and 1.505) and 4 synthesis temperatures (1175 °C, 1200 °C, 1250 °C, 1350 °C) detected a significant effect of the Ca/P molar ratio on d50 and d90 in number, and d10 and d50 in volume, and of the Ca/P molar ratio d10 and d90 in number, as well as d50 in volume. One may summarize the complex observations by stating that a lower synthesis temperature and a large Ca/P molar ratio led to finer single particles but more numerous large agglomerates.

The SSA values of the powders varied between 1.1 and 2.4 m^2/g (Fig. 5g–Table 4) without clear effect of Ca/P ratio or synthesis temperature. Nevertheless, a 2-way ANOVA analysis detected significant effects of the Ca/P molar ratio and the synthesis temperature on the SSA values. When comparing groups, only the powders sintered at 1175 °C had significantly higher SSA values than the powders sintered at 1350 °C ($p < 0.01$).

The reactivity of the powders was assessed using isothermal calorimetry data. The α-TCP aqueous pastes reached an exothermic peak 5–10 min after mixing, but the whole reaction lasted days (Figs. 6 and 7). Single curves suggest that an increase of the Ca/P molar ratio of the α-TCP powders reduced the time to reach the exothermic peak (Fig. 6a–c). Contrarily, the synthesis temperature did not seem to affect the results (Fig. 6e–g). When looking at the overall reaction, the powders produced with a Ca/P molar ratio inferior to 1.50 and a synthesis temperature of 1350 °C needed significantly more time to reach 100 % reaction rate (Fig. 6d–f). Statistically, both the Ca/P molar ratio and the synthesis temperature significantly affected the time to reach 10 %, 50 %, and 90 % of the reaction, as well as the time to reach the maximum. The fitting equations retrieved from the statistical model contained 1st order, 2nd order and 3rd order components, making any interpretation difficult. However, a Ca/P molar ratio below 1.50 significantly slowed the reaction, particularly for powders produced at 1350 °C (Fig. 7).

The reactivity of α-TCP powders is known to be affected by their SSA

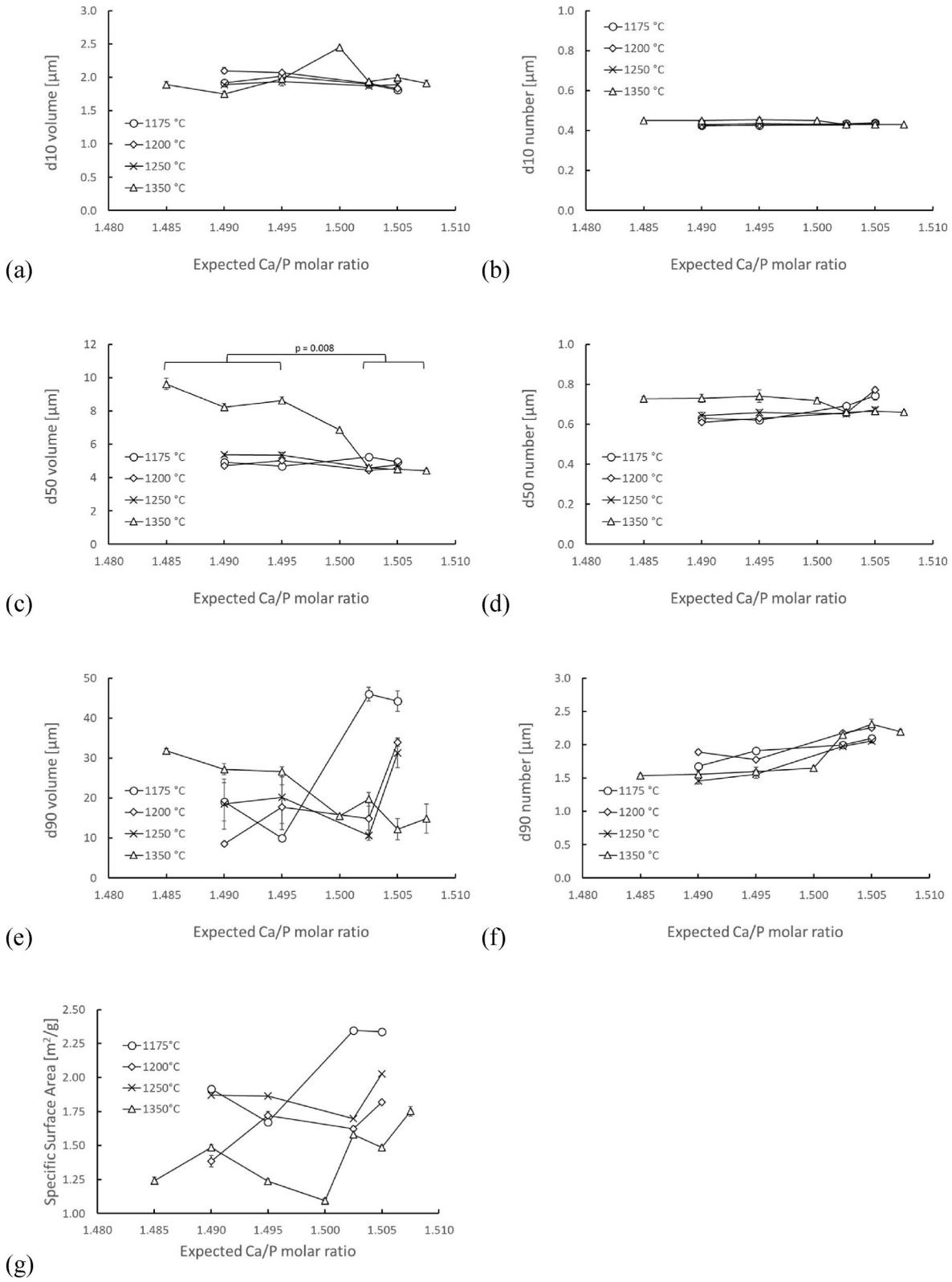

Fig. 5. Particle size distribution results are shown as (a,b) d10, (c,d) d50, (e,f) d90 values for the different synthesis temperatures and Ca/P molar ratios. The SSA values are plotted in (g). The error bars correspond to ± one standard deviation.

value and their ACP content [13]. Therefore, the isothermal calorimetry data was plotted as a function of the SSA value (Fig. 8) and the ACP content (Fig. S2). The results revealed that the reactivity was indeed increased with an increase of SSA: the time to reach 10 %, 50 % and 90 % of the total heat released during the reaction was significantly reduced (Fig. 8a,b,c). However, this statement was no longer valid at $p < 0.01$ for the 90 % released heat results when the results of the powders synthesized at 1350 °C and a Ca/P molar ratio lower than 1.50 were removed ($p = 0.04$; Fig. 8d). The height of the first exothermic peak was found to significantly increase with an increase of SSA (Fig. 8f), but its position

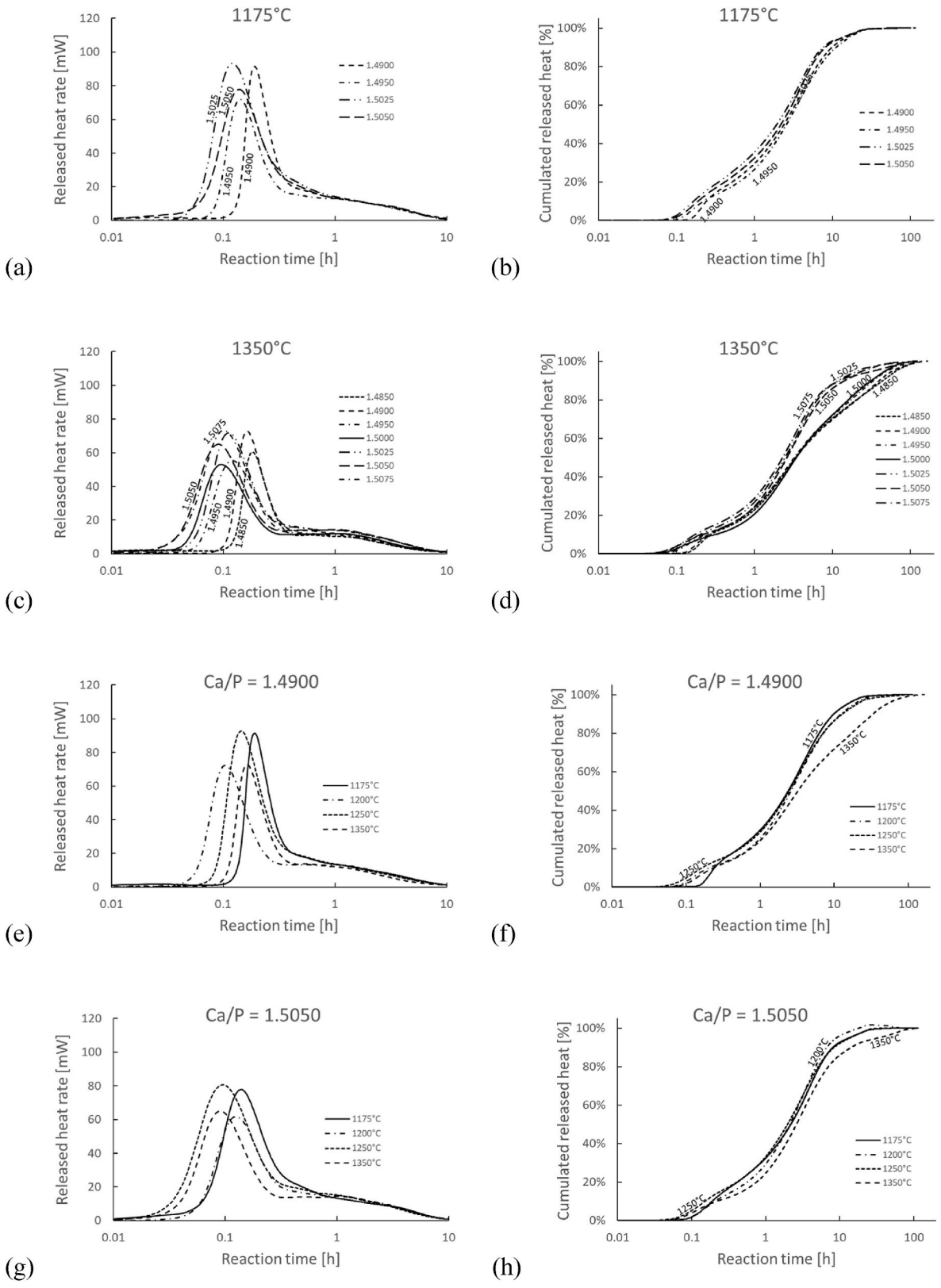

Fig. 6. Representative isothermal calorimetry curves for different synthesis temperatures and Ca/P molar ratios. The left column contains the released heat rate curves. The right column contains the cumulated released heat curves. The charts either show the results obtained at one synthesis temperature ((a,b) 1175 °C, (c,d) 1350 °C) or one Ca/P molar ratio ((e,f) Ca/P = 1.4900; (g,h) Ca/P = 1.5050).

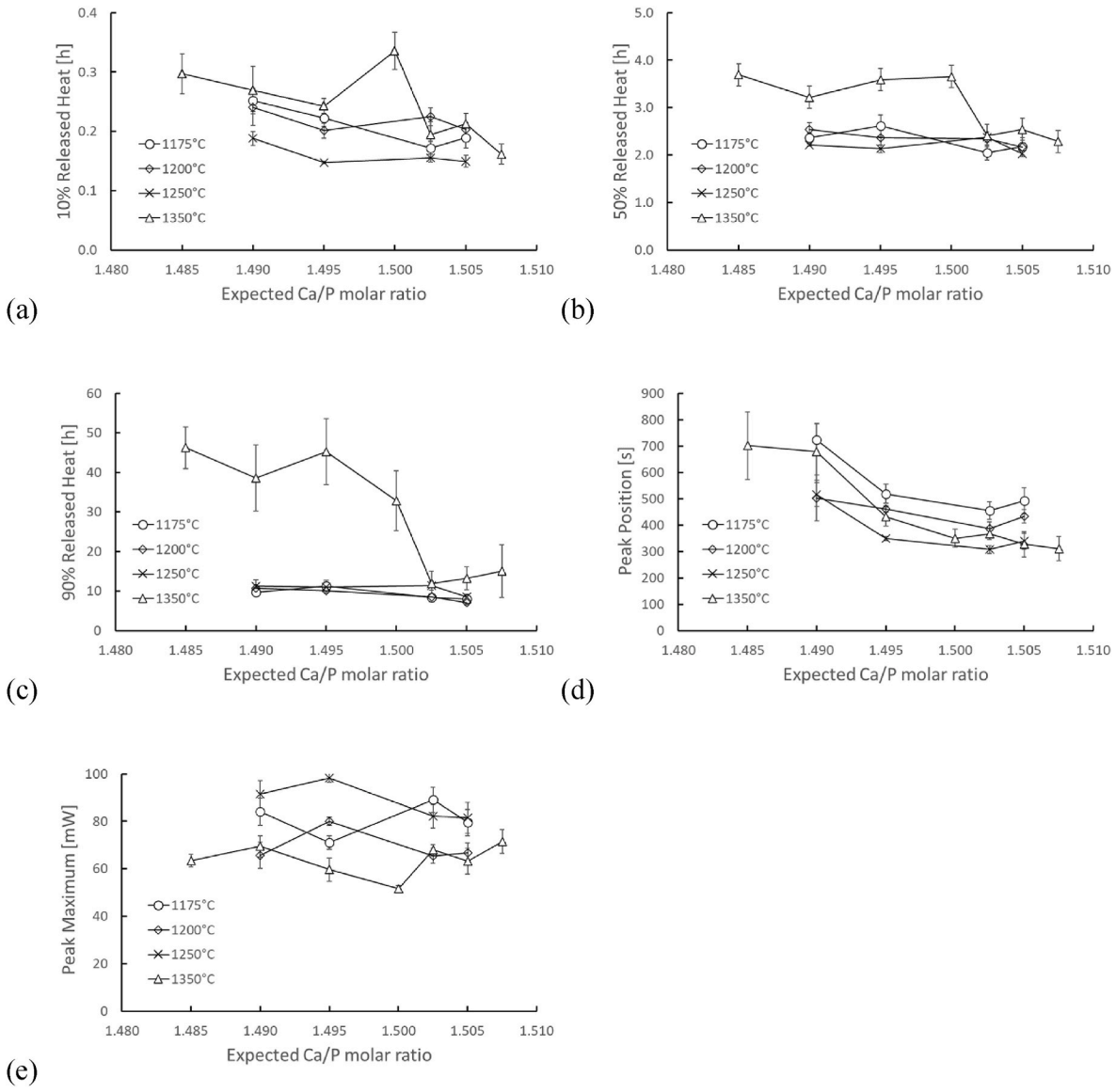

Fig. 7. Summary of the results obtained by isothermal calorimetry showing the effect of the Ca/P molar ratio and synthesis temperature on (a) 10 % released heat, (b) 50 % released heat, (c) 90 % released heat, (d) the peak position, and (e) the peak maximum. The error bars correspond to ± one standard deviation.

was not affected (Fig. 8e).

At first sight, the ACP content had only a significant effect on the height of the main exothermic peak (Figs. S2h and i), but not on its position, or on the time to reach 10 %, 50 %, and 90 % of the total released heat. However, after excluding the results obtained with the powders synthesized at 1350 °C and a Ca/P molar ratio below 1.50, there was a trend towards an increased reactivity at a higher ACP content (Figs. S2a–f). The effect was significant for the 50 % released heat values (Fig. S2d).

After the calorimetry experiments, some hardened cement samples were impregnated in a resin, polished and analyzed by SEM (Fig. 9). All samples contained the typical globular microstructure of α-TCP-based cements, namely apatite plate-like crystals surrounding and connecting mainly empty spherical pores left by the dissolution of α-TCP particles. Two peculiarities were detected. First, dense particles of up to ≈50 μm diameter were observed in cement samples produced with α-TCP powders sintered at 1350 °C and a Ca/P molar ratio below 1.50. Such dense particles were not detected in other cements, in particular cements made with α-TCP powders produced with the same Ca/P molar ratio, but a lower synthesis temperature (Fig. 10). Second, all cements contained agglomerates of up to 150 μm. These agglomerates appeared more numerous for samples with a Ca/P molar ratio above 1.50 and produced below 1350 °C (Figs. 9 and 10). Assuming that agglomerates were already present in the α-TCP powders, some cement pastes were produced in a speed mixer using milling balls. The resulting cement pastes became free of agglomerates (Fig. 11).

5. Discussion

ISO 13175-3, 13779-6 and ASTM F1088, F1185 standards consider that calcium phosphates are phase-pure when their crystalline purity exceeds 95 %. A simple conclusion would then be that the physico-chemical properties of such powders remain identical independently of the crystalline purity. However, recent results have shown that this is not true of β-TCP since the presence of less than 5 % β-CPP or HA strongly affected the crystalline structure as well as the physico-chemical and biological properties of β-TCP [18,19]. In this study, it was hypothesized that the presence of less than 5 % β-CPP or HA would affect the physico-chemical and hydraulic properties of α-TCP powders. The aim was then to produce α-TCP powders with various contents of

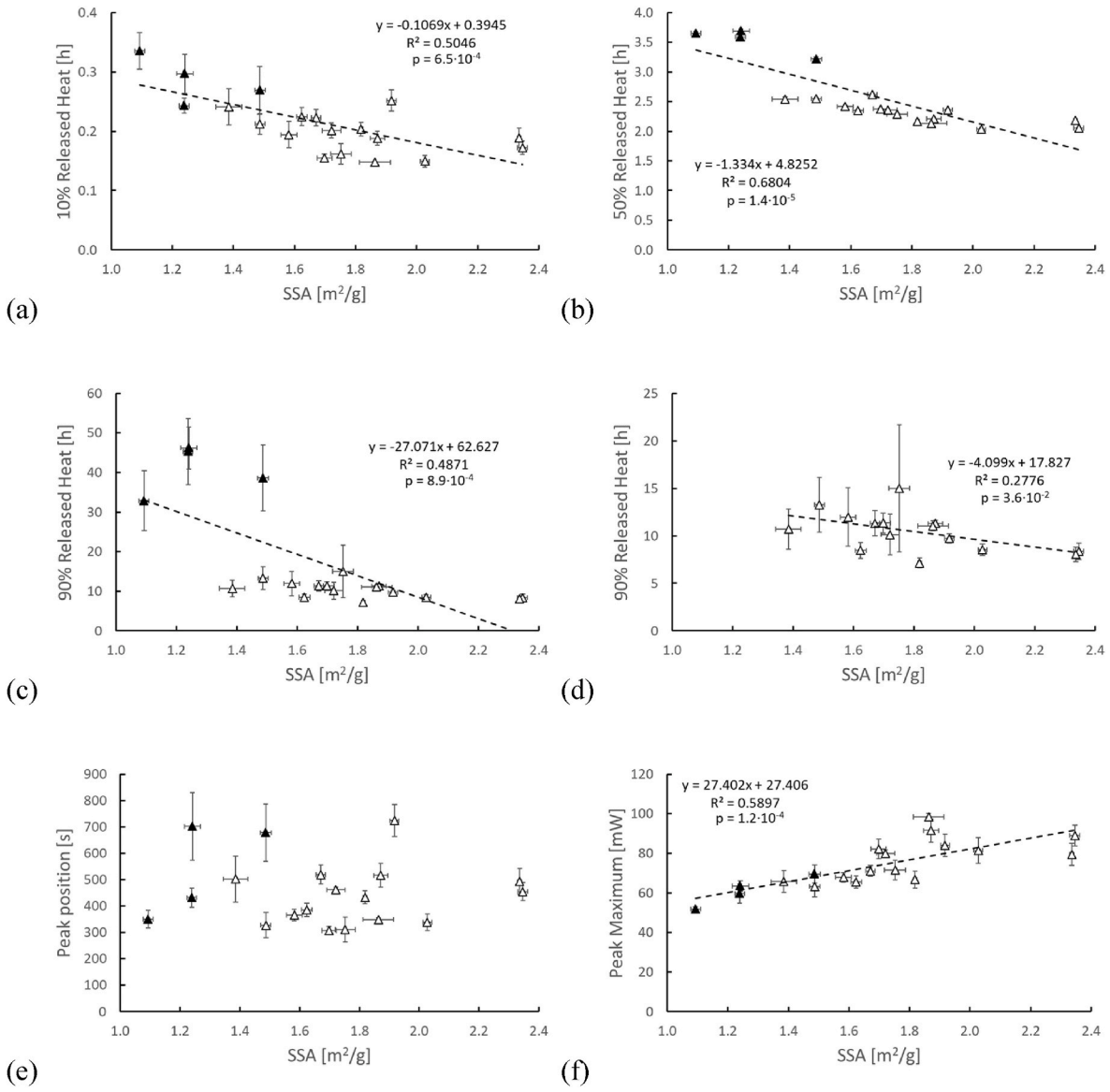

Fig. 8. Summary of the results obtained by isothermal calorimetry showing the correlation between the SSA and (a) 10 % released heat, (b) 50 % released heat, (c,d) 90 % released heat, (e) the peak position, and (f) the peak maximum. The difference between (c) and (d) is that the results obtained with powders synthesized at 1350 °C were removed in (d). The error bars correspond to ± one standard deviation. Linear regression lines are shown as well as their equations, the regression coefficients and the p values.

these two foreign phases and to characterize the powders and the cement pastes made with these powders.

The results showed that it is possible to produce crystalline α-TCP powders by solid-state reaction of CC and DCP in a chemically controllable and reproducible manner (Figs. 1 and 2; Table 3). This was expressed for example by a linear relationship between the measured and expected Ca/P molar ratio (Fig. 2e and f). An excellent agreement was found between XRD, XRF and ICP-MS measurement (Fig. 2f), in accordance with past studies [18]. Interestingly, the fit between the measured and expected Ca/P molar ratio was better at 1175 °C, 1200 °C, and 1250 °C than at 1350 °C (Fig. 2e). It was speculated that this could be due to the presence of amorphous CPP in the powders produced at 1350 °C. To check this hypothesis, the powders were calcined 24 h at 950 °C and characterized again by XRD. The Ca/P molar ratios differed by −0.0018 to 0.0021 from the initially measured values which can be expected considering the different specificity of the XRD Rietveld refinement quantifications of β-CPP in an α-TCP or β-TCP matrix, respectively (Fig. 2e). Furthermore, there was no trend suggesting that an amorphous CPP phase would have transformed into a crystalline phase.

Controlling the morphology of the powders by milling proved to be complicated. The SSA and PSD values seemed to vary erratically (Table 4). One would have expected to get higher SSA values with a lower synthesis temperature (Fig. 3, Fig. S1). However, significant differences were only found between the powders synthesized at 1175 °C and 1350 °C. Similarly, the Ca/P molar ratio had solely a significant effect on the d90 values of the PSD (Table 4). In fact, the only α-TCP powders that were significantly different from the other powders were those produced at 1350 °C and a Ca/P molar ratio below 1.50: they contained dense agglomerates with a mean size of 10–20 μm in diameter (Figs. 3 and 4, Fig. S1). The formation of these agglomerates can be ascribed to the formation of a liquid CPP phase above 1296 °C [20]. Accordingly, it is recommended to make sure that the Ca/P molar ratio of the α-TCP powder is slightly above a Ca/P molar ratio of 1.50 or that the synthesis temperature is below 1296 °C. The latter is often not possible because most raw materials contain Mg impurities which

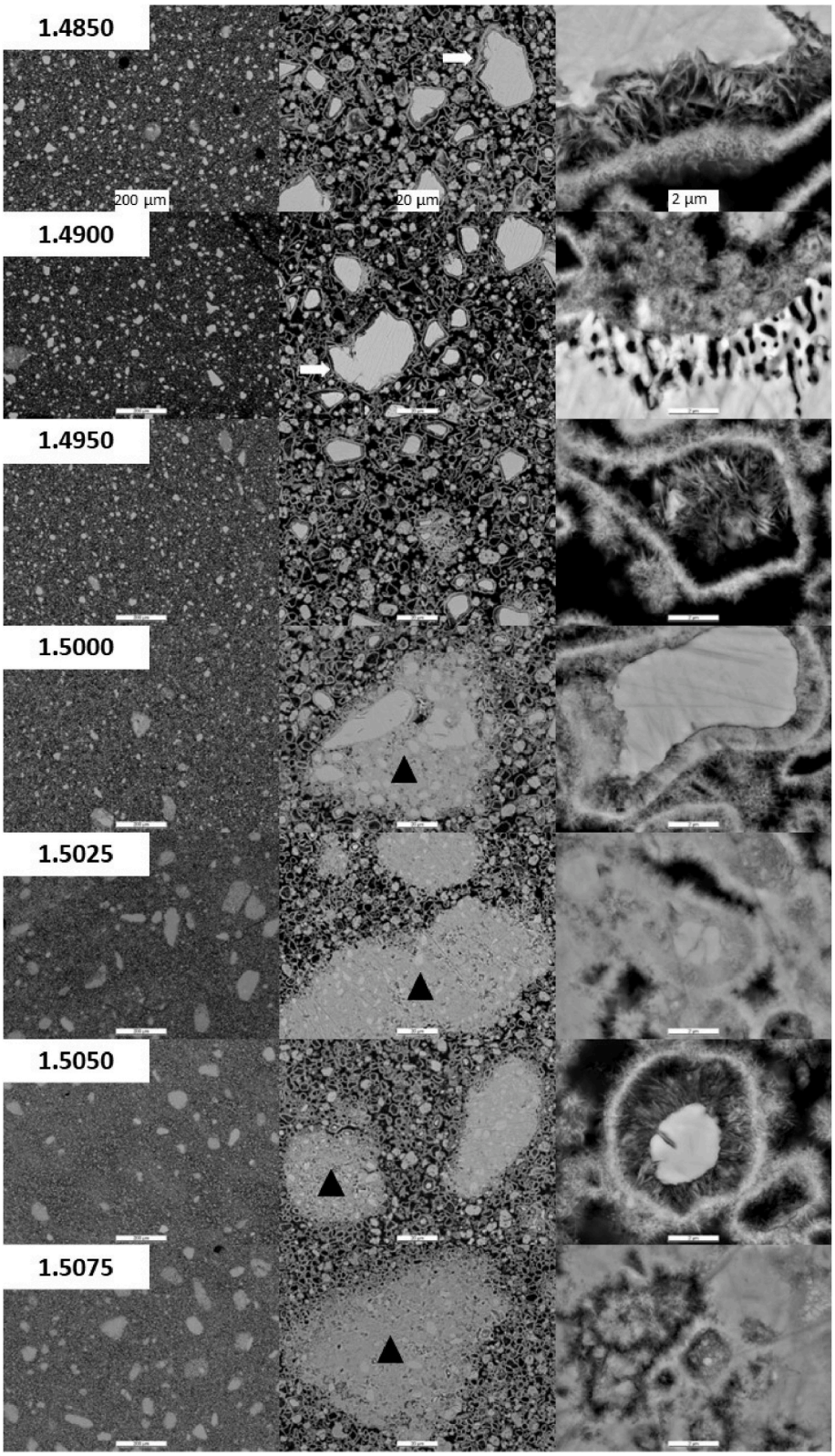

Fig. 9. SEM images of hardened cements produced with α-TCP powders synthesized at 1350 °C and different nominal Ca/P molar ratios. Three enlargements are shown per hardened cement sample. The scale bars have a width of 200, 20, and 2 µm, respectively (from left to right). Large dense and loose agglomerates are shown with a white arrow and a black triangle, respectively.

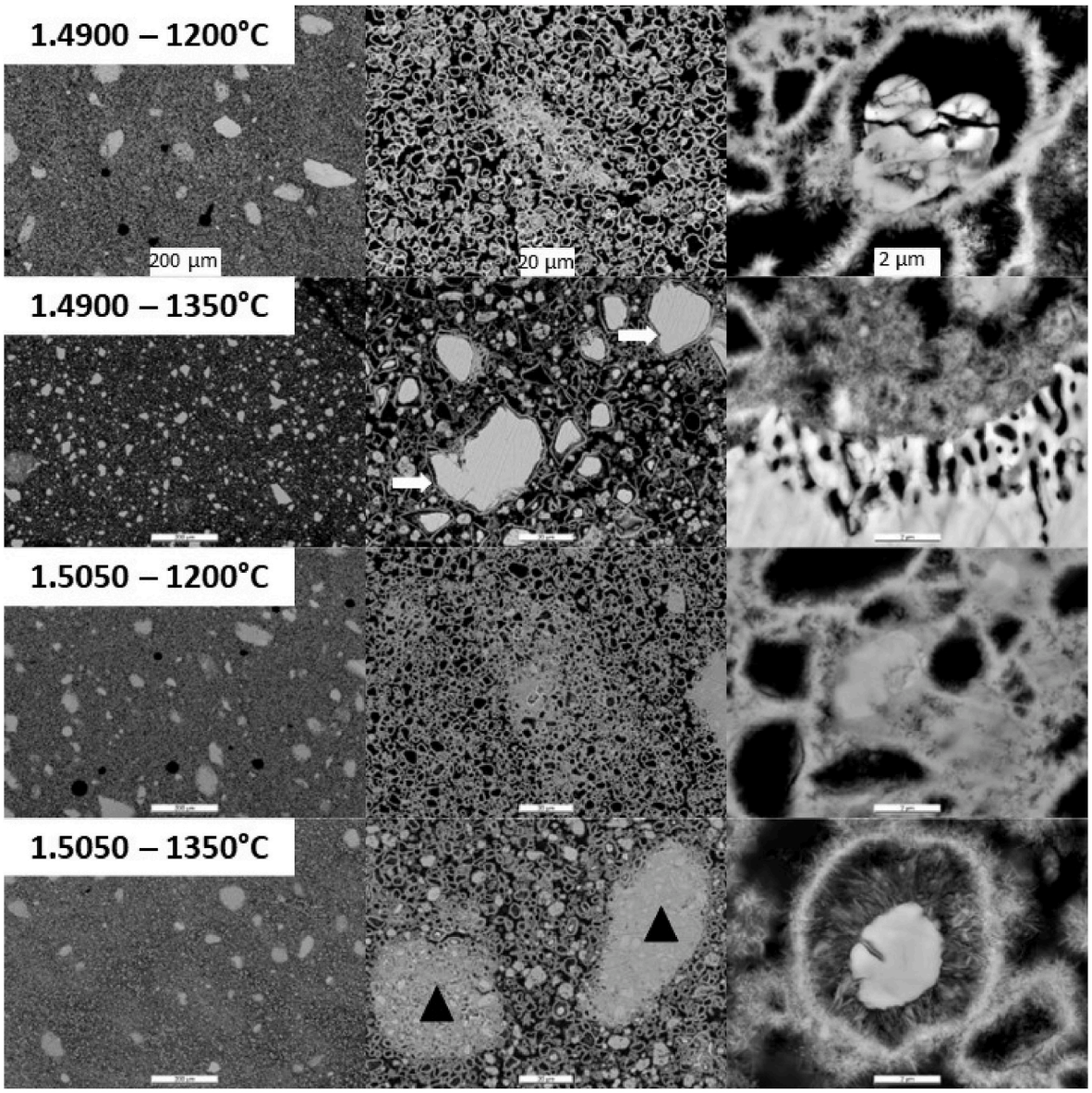

Fig. 10. SEM images of hardened cements produced with α-TCP powders synthesized at 1200 °C and 1350 °C and two different nominal Ca/P molar ratios, namely 1.4900 and 1.5050. Three enlargements are shown per hardened cement sample. The scale bars have a width of 200, 20, and 2 µm, respectively (from left to right). Large dense and loose agglomerates are shown with a white arrow and a black triangle, respectively.

increases the β-to α-TCP transition temperature and provokes the formation of stable β- TCP - α-TCP binary mixtures [26]. Also, it favors the formation of β-TCP during α-TCP cooling [21,27]. Accordingly, most researchers active in the field produce their α-TCP powders between 1300 °C and 1400 °C and quench them to prevent the formation of β-TCP during cooling [3,10,12,15,28–31].

Milling the α-TCP powders transformed a fraction of the crystalline phases into an amorphous calcium phosphate phase (ACP, defined as "not contributing to the α-TCP XRD signal"), which is more reactive than α-TCP. Prolonged milling can then be used to increase the hydraulic reactivity of β-TCP and α-TCP powders [31,32]. Here, the intention was not to produce large amounts of ACP, but just to deagglomerate the powders. The 15 min α-TCP milling time led to the formation of moderate amounts of ACP, i.e. 3–11 % ACP (Table 3). These amounts were limited enough to have only a moderate effect on the hydraulic reactivity of the α-TCP powders. The ACP content was neither a function of the Ca/P molar ratio, nor of the synthesis temperature (Fig. 2a). Since the reproducibility of the milling step is in our hands limited, it was speculated that the ACP could be a function of the SSA, but there was only a weak positive correlation between ACP and SSA ($r^2 = 0.1$).

Lowering the synthesis temperature did lead to finer powders and to a slight increase of SSA (Fig. 5). However, the main effect contributing to a reduction of α-TCP particle size was related to the Ca/P molar ratio: the powders were finer and had higher SSA values above a Ca/P molar ratio of 1.50.

The minute changes of composition of the α-TCP powders produced with various Ca/P molar ratios and synthesis temperature resulted in surprisingly large changes in powder reactivity (Figs. 6 and 7. Fig. S2). For example, the time to reach 90 % released heat was increased fourfold when the powders with a Ca/P molar ratio below 1.50 were sintered at 1350 °C (Fig. 7c). Similarly, the position of the largest exothermic peak during α-TCP hydraulic reaction was decreased twofold with an increase of Ca/P molar ratio (Fig. 7d). However, it was difficult to distinguish a clear effect of the synthesis temperature or Ca/P molar ratio. To understand these differences, the various values retrieved from the calorimetry experiments were plotted as a function of the two known properties affecting the reactivity of α-TCP-based CPCs, namely the SSA value [9–11] and the ACP content [9,13–16]. Fig. 8a confirmed that the

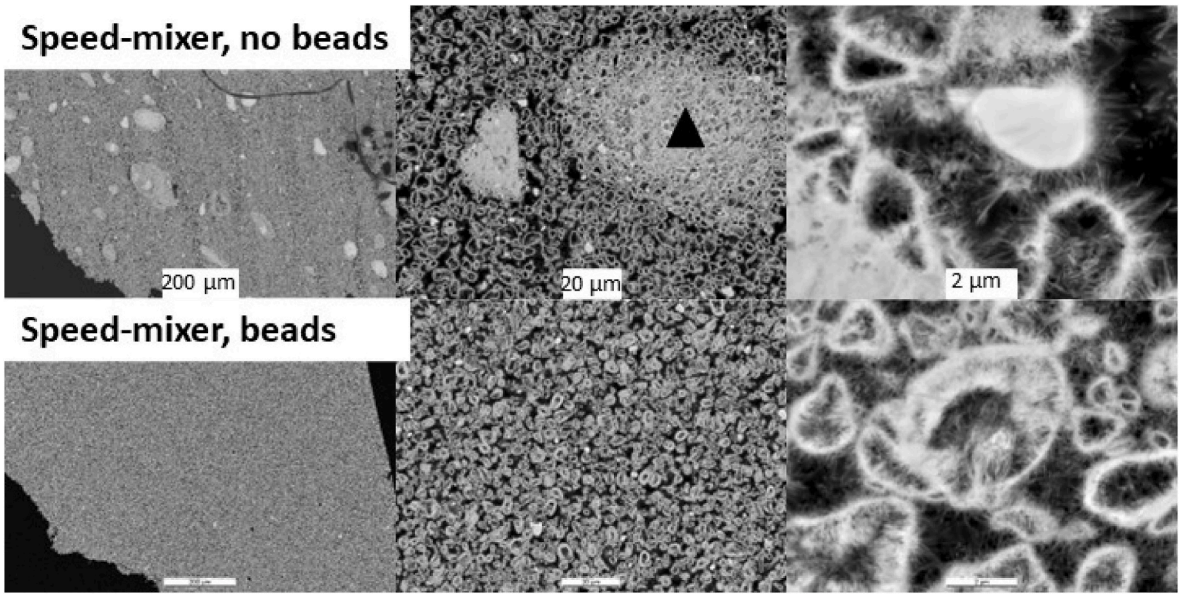

Fig. 11. SEM images of hardened cements produced with α-TCP powders synthesized at 1250 °C and a Ca/P molar ratio of 1.5025. Three enlargements are shown per hardened cement sample. The scale bars have a width of 200, 20, and 2 µm, respectively (from left to right). The large loose agglomerates seen in cement samples mixed with a spatula (black triangle) are not seen in cement samples mixed with the speed-mixer and zirconia beads.

SSA value significantly affected the time to reach 10 % released heat, which is generally considered to be a proxy for the setting time [16]. Higher SSA values also led to larger exothermic peaks (Fig. 8f) and a faster global reaction (Fig. 8a–d) [10,11]. The ACP content had a more limited effect on the reactivity of the powders than the SSA value (Fig. S2). Nevertheless, the height of the main exothermic peak was significantly increased with an increase in ACP content (Figs. S2h and i), in accordance to the fact that the first phase that reacts during α-TCP hydrolysis is ACP [13]. Also, there was a tendency for the powders to react faster with a higher ACP content.

Contrary to most studies, the microstructure of the hardened cements was not observed on broken surfaces, but on polished surfaces (Figs. 9–11). This allowed a more in-depth analysis of the microstructure [33]. The images suggest that the dissolution products of α-TCP particles precipitate mostly at the surface of the α-TCP particles, thus leaving a hole in the center of the location where the α-TCP particles were [33]. Partly reacted dense α-TCP particles were clearly visible in samples produced with α-TCP powders synthesized at 1350 °C and a nominal Ca/P molar ratio below 1.500 (Fig. 9). These particles were very slow to react due to the diffusion-controlled reaction mechanism [34], as evidenced by the long time needed to reach 90 % of the reaction (Figs. 7 and 8). By using a synthesis temperature below the melting temperature of α-CPP (1296 °C), the dense α-TCP agglomerates disappeared, and the time for the cement to reach 90 % of released heat was drastically reduced (Figs. 8 and 9). More translucent (= less dense) agglomerates were observed in all hardened CPCs except when the cements were mixed in a static mixer with dense zirconia beads (Figs. 9–11). The presence of these agglomerates was then attributed to the presence of α-TCP powder agglomerates in the α-TCP powders.

Ideally, α-TCP powders should be fine and deagglomerated to be highly reactive and injectable. Here, the use of a synthesis temperature below the melting temperature of α-CPP (1290 °C) and a Ca/P molar ratio above 1.50 had a favorable effect to remove dense agglomerates (Figs. 9 and 10). However, large porous agglomerates were still found in the powders produced at lower synthesis temperatures. Neither the manual paste mixing using a spatula nor the mechanical mixing using the Speed Mixer without beads were intensive enough to remove these agglomerates (Fig. 11). It is unclear at this point when these agglomerates form and how their formation can be prevented.

The results confirmed that α-TCP powders with higher SSA values and ACP content were more reactive (Fig. 8). However, relatively large changes of reactivity were found between powders with similar SSA values. Part of these effects could be explained by a difference of Ca/P molar ratio (a lower ratio leading to a lower reactivity), but not all. At this point, the origin of these differences is unclear. Importantly, no special attention was paid to storing the powders in controlled atmosphere. Even though Espanol et al. [35] did not detect any change of α-TCP reactivity after 3 weeks incubation in 80 % relative humidity conditions, they observed that part of the adsorbed water was irreversibly bound to α-TCP particle surface. It is known that α-TCP reactivity can be increased by humidifying them temporarily [36].

6. Conclusion

This study significantly advances our understanding of α-tricalcium phosphate (α-TCP) powders, revealing that minor phase impurities below 5 %, such as β-CPP or HA, can substantially influence the crystalline structure, and physico-chemical properties of calcium phosphate materials. Contrary to the standards set by ISO and ASTM, which suggest that crystalline purity above 95 % should yield identical material properties, the findings highlight the critical impact of synthesis conditions on the properties of α-TCP powders. The study reveals that α-TCP powders should be produced below the α-CPP melting temperature of 1296 °C to prevent the formation of dense agglomerates and a low reactivity. An alternative consists in using a slight excess of Ca.

Experimental results demonstrated the ability to produce crystalline α-TCP powders with precise control over the Ca/P molar ratio and highlighted the role of synthesis temperature in optimizing the physico-chemical characteristics and reactivity of these powders. Moreover, the study underlines the challenges in controlling powder morphology through milling, showing how it unpredictably affects specific surface area and particle size distribution, thus influencing the reactivity of the powders. This represents a challenge for α-TCP based cement applications where the setting time needs to be tightly controlled.

The investigation provides key insights into optimizing α-TCP powder synthesis and processing techniques, emphasizing the importance of temperature and Ca/P molar ratio in enhancing the hydraulic reactivity of calcium phosphate cements. By meticulously controlling synthesis parameters, this research paves the way for developing more effective biomedical materials for bone regeneration, challenging existing purity

standards and offering new perspectives on material design and application in the biomedical field.

CRediT authorship contribution statement

Marc Bohner: Conceptualization, Data curation, Formal analysis, Investigation, Methodology, Project administration, Resources, Supervision, Writing – original draft, Writing – review & editing. **Fabrizio Bigolin:** Investigation. **Isabelle Bohner:** Investigation. **Thomas Imwinkelried:** Investigation, Methodology, Writing – review & editing. **Yassine Maazouz:** Conceptualization, Formal analysis, Investigation, Methodology, Writing – original draft, Writing – review & editing. **Pascal Michel:** Investigation. **Christoph Stähli:** Formal analysis, Investigation, Methodology. **Yves Viecelli:** Investigation. **Nicola Döbelin:** Conceptualization, Formal analysis, Investigation, Methodology, Supervision, Writing – original draft, Writing – review & editing.

Declaration of competing interest

The authors declare that they have no known competing financial interests or personal relationships that could have appeared to influence the work reported in this paper.

Appendix A. Supplementary data

Supplementary data to this article can be found online at https://doi.org/10.1016/j.oceram.2024.100647.

References

[1] H. Monma, T. Kanazawa, The hydration of a-tricalcium phosphate, Yogyo-Kyokai-Shi 84 (4) (1976) 209–213.

[2] B.R. Constantz, I.C. Ison, M.T. Fulmer, R.D. Poser, S.T. Smith, M. VanWagoner, J. Ross, S.A. Goldstein, J.B. Jupiter, D.I. Rosenthal, Skeletal repair by in situ formation of the mineral phase of bone, Science 267 (1995) (1979) 1796–1799. http://www.ncbi.nlm.nih.gov/entrez/query.fcgi?cmd=Retrieve&db=PubMed&dopt=Citation&list_uids=7892603.

[3] K.S. TenHuisen, P.W. Brown, Formation of calcium-deficient hydroxyapatite from alpha-tricalcium phosphate, Biomaterials 19 (1998) 2209–2217. http://www.ncbi.nlm.nih.gov/entrez/query.fcgi?cmd=Retrieve&db=PubMed&dopt=Citation&list_uids=9884062.

[4] S.B. Goodman, T.W. Bauer, D. Carter, P.P. Casteleyn, S.A. Goldstein, R.F. Kyle, S. Larsson, C.J. Stankewich, M.F. Swiontkowski, A.F. Tencer, D.N. Yetkinler, R. D. Poser, Norian SRS cement augmentation in hip fracture treatment. Laboratory and initial clinical results, Clin. Orthop. Relat. Res. (1998) 42–50. http://www.ncbi.nlm.nih.gov/entrez/query.fcgi?cmd=Retrieve&db=PubMed&dopt=Citation&list_uids=9553532.

[5] D.N. Yetkinler, R.T. McClellan, E.S. Reindel, D. Carter, R.D. Poser, Biomechanical comparison of conventional open reduction and internal fixation versus calcium phosphate cement fixation of a central depressed tibial plateau fracture, J. Orthop. Trauma 15 (2001) 197–206. http://www.ncbi.nlm.nih.gov/entrez/query.fcgi?cmd=Retrieve&db=PubMed&dopt=Citation&list_uids=11265011.

[6] P. Kopylov, K. Runnqvist, K. Jonsson, P. Aspenberg, Norian SRS versus external fixation in redisplaced distal radial fractures. A randomized study in 40 patients, Acta Orthop. Scand. 70 (1999) 1–5. http://www.ncbi.nlm.nih.gov/entrez/query.fcgi?cmd=Retrieve&db=PubMed&dopt=Citation&list_uids=10191737.

[7] M. Nakano, N. Hirano, H. Ishihara, Y. Kawaguchi, H. Watanabe, K. Matsuura, Calcium phosphate cement-based vertebroplasty compared with conservative treatment for osteoporotic compression fractures: a matched case-control study, J. Neurosurg. Spine 4 (2006) 110–117. http://www.ncbi.nlm.nih.gov/entrez/query.fcgi?cmd=Retrieve&db=PubMed&dopt=Citation&list_uids=16506477.

[8] M. Bohner, G. Baroud, Injectability of calcium phosphate pastes, Biomaterials 26 (2005) 1553–1563. http://www.ncbi.nlm.nih.gov/entrez/query.fcgi?cmd=Retrieve&db=PubMed&dopt=Citation&list_uids=15522757.

[9] E.B. Montufar, Y. Maazouz, M.P. Ginebra, Relevance of the setting reaction to the injectability of tricalcium phosphate pastes, Acta Biomater. 9 (2013) 6188–6198, https://doi.org/10.1016/j.actbio.2012.11.028.

[10] M.P. Ginebra, F.C.M. Driessens, J.A. Planell, Effect of the particle size on the micro and nanostructural features of a calcium phosphate cement: a kinectic analysis, Biomaterials 25 (2004) 3453–3462.

[11] C. Durucan, P.W. Brown, Kinetic model for alpha-tricalcium phosphate hydrolysis, J. Am. Ceram. Soc. 85 (2002) 2013–2018.

[12] M. Espanol, R.A. Perez, E.B. Montufar, C. Marichal, A. Sacco, M.P. Ginebra, Intrinsic porosity of calcium phosphate cements and its significance for drug delivery and tissue engineering applications, Acta Biomater. 5 (2009) 2752–2762. http://www.ncbi.nlm.nih.gov/entrez/query.fcgi?cmd=Retrieve&db=PubMed&dopt=Citation&list_uids=19357005.

[13] K. Hurle, J. Neubauer, M. Bohner, N. Doebelin, F. Goetz-Neunhoeffer, Effect of amorphous phases during the hydraulic conversion of α-TCP into calcium-deficient hydroxyapatite, Acta Biomater. 10 (2014) 3931–3941, https://doi.org/10.1016/j.actbio.2014.03.017.

[14] M. Bohner, R. Luginbühl, C. Reber, N. Doebelin, G. Baroud, E. Conforto, A physical approach to modify the hydraulic reactivity of alpha-tricalcium phosphate powder, Acta Biomater. 5 (2009) 3524–3535, https://doi.org/10.1016/j.actbio.2009.05.024.

[15] C.L. Camire, U. Gbureck, W. Hirsiger, M. Bohner, Correlating crystallinity and reactivity in an alpha-tricalcium phosphate, Biomaterials 26 (2005) 2787–2794. http://www.ncbi.nlm.nih.gov/entrez/query.fcgi?cmd=Retrieve&db=PubMed&dopt=Citation&list_uids=15603774.

[16] M. Bohner, T.J. Brunner, W.J. Stark, Controlling the reactivity of calcium phosphate cements, J. Mater. Chem. 18 (2008) 5669–5675.

[17] C. Durucan, P.W. Brown, Reactivity of alpha-tricalcium phosphate, J. Mater. Sci. 37 (1999) 963–969.

[18] B. Le Gars Santoni, L. Niggli, G.A. Sblendorio, D.T.L. Alexander, C. Stähli, P. Bowen, N. Döbelin, M. Bohner, Chemically pure β-tricalcium phosphate powders: evidence of two crystal structures, J. Eur. Ceram. Soc. 41 (2021) 1683–1694, https://doi.org/10.1016/j.jeurceramsoc.2020.09.055.

[19] B. Le Gars Santoni, L. Niggli, S. Dolder, O. Loeffel, G.A. Sblendorio, R. Heuberger, Y. Maazouz, C. Stähli, N. Döbelin, P. Bowen, W. Hofstetter, M. Bohner, Effect of minor amounts of β-calcium pyrophosphate and hydroxyapatite on the physico-chemical properties and osteoclastic resorption of β-tricalcium phosphate cylinders, Bioact. Mater. 10 (2022) 222–235, https://doi.org/10.1016/j.bioactmat.2021.09.003.

[20] P. Hudon, I.H. Jung, Critical evaluation and thermodynamic Optimization of the CaO-P2O5 system, Metall. Mater. Trans. B 46 (2014) 494–522, https://doi.org/10.1007/s11663-014-0193-x.

[21] P.M.C. Torres, J.C.C. Abrantes, A. Kaushal, S. Pina, N. Döbelin, M. Bohner, J.M. F. Ferreira, Influence of Mg-doping, calcium pyrophosphate impurities and cooling rate on the allotropic α <-> β-tricalcium phosphate phase transformations, J. Eur. Ceram. Soc. 36 (2016) 817–827, https://doi.org/10.1016/j.jeurceramsoc.2015.09.037.

[22] R.G. Carrodeguas, S. De Aza, α-Tricalcium phosphate: synthesis, properties and biomedical applications, Acta Biomater. 7 (2011) 3536–3546, https://doi.org/10.1016/j.actbio.2011.06.019.

[23] N. Doebelin, Y. Maazouz, R. Heuberger, M. Bohner, A.A. Armstrong, A.J. Wagoner Johnson, C. Wanner, A thermodynamic approach to surface modification of calcium phosphate implants by phosphate evaporation and condensation, J. Eur. Ceram. Soc. 40 (2020) 6095–6106.

[24] N. Doebelin, R. Kleeberg, Profex: a graphical user interface for the Rietveld refinement program BGMN, J. Appl. Crystallogr. 48 (2015) 1573–1580, https://doi.org/10.1107/S1600576715014685.

[25] I.C. Madsen, N.V.Y. Scarlett, Quantitative phase analysis, in: R.E. Dinnebier, S.J. L. Billinge (Eds.), Powder Diffraction: Theory and Practice, The Royal Society of Chemistry, Cambridge, 2008, pp. 298–331, https://doi.org/10.1039/9781847558237-00298.

[26] R.G. Carrodeguas, A.H. De Aza, X. Turrillas, P. Pena, S. De Aza, New approach to the beta-alpha polymorphic transformation in magnesium-substituted tricalcium phosphate and its practical implications, J. Am. Ceram. Soc. 91 (2008) 1281–1286. http://www.scopus.com/scopus/inward/record.url?eid=2-s2.0-41549162406&partnerID=40&rel=R8.0.0.

[27] M. Frasnelli, V.M. Sglavo, Effect of Mg2+ doping on beta-alpha phase transition in tricalcium phosphate (TCP) bioceramics, Acta Biomater. 33 (2016) 283–289, https://doi.org/10.1016/j.actbio.2016.01.015.

[28] E. Fernandez, M.P. Ginebra, M.G. Boltong, F.C. Driessens, J. Ginebra, E.A. De Maeyer, R.M. Verbeeck, J.A. Planell, Kinetic study of the setting reaction of a calcium phosphate bone cement, J. Biomed. Mater. Res. 32 (1996) 367–374. http://www.ncbi.nlm.nih.gov/entrez/query.fcgi?cmd=Retrieve&db=PubMed&dopt=Citation&list_uids=8897141.

[29] E. Fernandez, F.J. Gil, M.P. Ginebra, F.C.M. Driessens, J.A. Planell, S.M. Best, Production and characterization of new calcium phosphate bone cements in the CaHPO4-a-Ca3(PO4)2 system: pH, workability, and setting times, J. Mater. Sci. Mater. Med. 10 (1999) 223–230.

[30] G. Cicek, E.A. Aksoy, C. Durucan, N. Hasirci, Alpha-tricalcium phosphate (α-TCP): solid state synthesis from different calcium precursors and the hydraulic reactivity, J. Mater. Sci. Mater. Med. 22 (2011) 809–817.

[31] U. Gbureck, J.E. Barralet, L. Radu, H.G. Klinger, R. Thull, Amorphous alpha-tricalcium phosphate: preparation and aqueous setting reaction, J. Am. Ceram. Soc. 87 (2004) 1126–1132.

[32] U. Gbureck, O. Grolms, J.E. Barralet, L.M. Grover, R. Thull, Mechanical activation and cement formation of beta-tricalcium phosphate, Biomaterials 24 (2003) 4123–4131. http://www.ncbi.nlm.nih.gov/entrez/query.fcgi?cmd=Retrieve&db=PubMed&dopt=Citation&list_uids=12853242.

[33] M. Le Ferrec, C. Mellier, F. Lefèvre, F. Boukhechba, P. Janvier, G. Montavon, J. Bouler, O. Gauthier, B. Bujoli, In vivo resorption of injectable apatitic calcium phosphate cements: critical role of the intergranular microstructure, J. Biomed. Mater. Res. B Appl. Biomater. 108 (2020) 367–376, https://doi.org/10.1002/jbm.b.34395.

[34] M. Bohner, Reactivity of calcium phosphate cements, J. Mater. Chem. 17 (2007) 3980–3986.
[35] M. Espanol, E. Davis, E. Meslet, G. Mestres, E.B. Montufar, M.-P. Ginebra, Effect of moisture on the reactivity of alpha-tricalcium phosphate, Ceram. Int. 49 (2023) 18228–18237, https://doi.org/10.1016/j.ceramint.2023.02.193.
[36] A. Butscher, M. Bohner, N. Doebelin, L. Galea, O. Loeffel, R. Müller, Moisture based three-dimensional printing of calcium phosphate structures for scaffold engineering, Acta Biomater. 9 (2013) 5369–5378, https://doi.org/10.1016/j.actbio.2012.10.009.